A novel framework to intercept GPS-denied, bomb-carrying, non-military, kamikaze drones: Towards protecting critical infrastructures

Athanasios N. Skraparlis [a, *], Klimis S. Ntalianis [a], Nicolas Tsapatsoulis [b]

[a] University of West Attica, 28 Agiou Spyridonos str., Athens 12241, Greece
[b] Cyprus University of Technology, Limassol 3036, Cyprus

ARTICLE INFO

ABSTRACT

Protection of urban critical infrastructures (CIs) from GPS-denied, bomb-carrying kamikaze drones (G-B-KDs) is very challenging. Previous approaches based on drone jamming, spoofing, communication interruption and hijacking cannot be applied in the case under examination, since G-B-KDs are uncontrolled. On the other hand, drone capturing schemes and electromagnetic pulse (EMP) weapons seem to be effective. However, again, existing approaches present various limitations, while most of them do not examine the case of G-B-KDs. This paper, focuses on the aforementioned under-researched field, where the G-B-KD is confronted by two defensive drones. The first neutralizes and captures the kamikaze drone, while the second captures the bomb. Both defensive drones are equipped with a net-gun and an innovative algorithm, which, among others, estimates the locations of interception, using a real-world trajectory model. Additionally, one of the defensive drones is also equipped with an EMP weapon to damage the electronics equipment of the kamikaze drone and reduce the capturing time and the overall risk. Extensive simulated experiments and comparisons to state-of-art methods, reveal the advantages and limitations of the proposed approach. More specifically, compared to state-of-art, the proposed approach improves: (a) time to neutralize the target by at least 6.89%, (b) maximum number of missions by at least 1.27% and (c) total cost by at least 5.15%.

1. Introduction

A nation's productivity, quality of life and economic progression, heavily depend on CIs. Their importance is such that their inability or destruction could have a severe impact on national defense, economic stability, and public safety. For these reasons, CIs often become top-level targets. Well-known serious incidents include: (a) the UAV attack on Aramco's Abqaiq and Khurais facilities in August 2019, resulting in the disruption of 50% of the Kingdom of Saudi Arabia's primary asset, the world's largest oil production center. A swarm of 10 UAVs carried out this severe attack [1], (b) the January 2023 bomb-carrying UAVs' attack on an Iranian defense factory in the central city of Isfahan. The attack caused some damage at the plant [2], (c) the December 2018 flights disruption at Gatwick Airport, due to UAVs. The Airport suspended all flights to avoid collision between UAVs and aircraft. The incident led to the diversion or cancellation of approximately 1000 flights, impacting around 140,000 passengers. The investigation incurred a cost of £800,000 [3].

In our previous research [4], neighboring CIs are considered, which are endangered by trucks, carrying explosive substances. Threat analysis covers three different scenarios and Voronoi tessellation is incorporated to limit the area of assessment. This paper significantly extends [4] by confronting aerial instead of ground threats. In particular it focuses on intercepting G-B-KDs, to protect urban CIs, where typically strict restrictions are applied on the use of anti-aircraft weapons, including missiles. G-B-KDs achieve self-navigation without GPS or remote control (using e.g. pre-installed satellite maps, cameras and artificial intelligence). It is also assumed that they are rigged with explosives and carry a releasable bomb, while their mission is to cause maximum damage to the target CI.

In the literature, several works have focused on civilian drones' stopping strategies, based on jamming, spoofing, communication interruption or hijacking [5]. However, these schemes cannot be

* Corresponding author.
E-mail address: askraparlis@uniwa.gr (A.N. Skraparlis).
Peer review under responsibility of China Ordnance Society

A.N. Skraparlis, K.S. Ntalianis and N. Tsapatsoulis

applied in the case under examination, since G-B-KDs are uncontrolled. On the other hand, drone capturing schemes and EMP weapons can be effective. However, existing approaches either examine net/catching technologies or EMP to neutralize drones, without combining both. Furthermore, locations of interception are estimated in few approaches. Additionally, most schemes do not consider drones carrying bombs.

The proposed scheme is classified among drone capturing approaches, incorporating EMP, a net gun and a novel interception algorithm. In particular, two defensive drones (DDs) confront the G-B-KD. The first DD neutralizes and captures the G-B-KD, while the second DD captures the bomb. To succeed to their missions: (a) both DDs are equipped with a net-gun and run an innovative algorithm, which, among other, estimates the most likely trajectory locations to intercept and capture the bomb and the G-B-KD and (b) the first DD is also equipped with an EMP weapon to damage the electronics of the G-B-KD.

To summarize, the major contributions of this paper are:

- It examines the under-researched field of kamikaze drones carrying releasable bombs of different Relative Effectiveness Factors in urban environments, which has not been comprehensively studied in the literature.
- It investigates DDs equipped both with net-guns and EMP, in contrast to existing methods, which propose either a net/catching technology or EMP.
- It establishes a real-world model of the trajectory of the bomb and G-B-KD in case of free fall with air resistance.
- It proposes a novel algorithm, which, among others, estimates the locations of interception, using the real-world trajectory model.
- It provides simulated experiments, using real world parameters, while it carries out extensive comparisons to state-of-art methods.

The remainder is organized as follows: Section 2 presents background information. Section 3 explores related work. Section 4 outlines the proposed scheme, with simulated results and comparisons presented in Section 5. Lastly, Section 6 concludes the paper, highlighting potential future research.

2. Background

2.1. Definitions and background information

- Atmospheric pressure at sea level: 1 atm ($=$14.696 psi).
- Gauge pressure: pressure variance between a supply tank and the surrounding air (disregarding atmospheric pressure).
- Overpressure: pressure resulting from a shock wave exceeding the standard atmospheric pressure.
- Relative Effectiveness Factor (REF): provides a comparison of a substance's explosive capability to the respective explosive capability of Trinitrotoluene.

Table 1 [6] outlines the anticipated infrastructure damage based on overpressure. As observed, overpressures >1 may cause serious damage.

2.2. REF of various substances

Let S_i, $i = 1, 2, \cdots, n$, be an explosive substance. Let also $REF(S_i^u)$ express the *REF* per unit for each different S_i. Table 2 [7–10] provides the *REF* for various S_i's.

For example, if 1 kg of Trinitrotoluene demolishes a wall, then 0.42 kg (1.0/2.38) of octanitrocubane can achieve the same result.

2.3. Blast-waves

When an S_i explodes it produces a shock wave, which is depicted in Fig. 1 [11] (pressure-time waveform). The ideal waveform is visualized for a distance r_c from the center of the blast. The atmospheric pressure is denoted by P_{atm}, while the positive phase, the negative phase and the time of arrival are denoted by t_{pos}, t_{neg} and t_{ar} respectively. Additionally, pim_o denotes the positive incident impulse, P_{ov} denotes the peak overpressure and P_{un} denotes the peak underpressure. Then [11]

$$P(t) = P_{atm} + P_{ov}\frac{(t_{pos} - t)}{t_{pos}}, 0 < t \le t_{pos} \tag{1}$$

and more accurately [11]

$$P(t) = P_{atm} + P_{ov}e^{-\delta t} \tag{2}$$

where the decay rate is denoted by δ, while t_{ar} is used to start measuring t.

Moreover, PR_f that denotes the proximity factor can be calculated by [12,13].

$$PR_f = \frac{r_c}{\sqrt[3]{M_e}} \tag{3}$$

where M_e denotes the mass of the explosive in kilograms (Trinitrotoluene). Blast-waves have been extensively studied and this paper adopts the formula of Ref. [14], which covers all distances

$$P_{ov} = P_{atm}\frac{808\left[1 + \left(\frac{PR_f}{4.5}\right)^2\right]}{\sqrt{\left[1 + \left(\frac{PR_f}{0.048}\right)^2\right]} \cdot \sqrt{\left[1 + \left(\frac{PR_f}{0.32}\right)^2\right]} \cdot \sqrt{\left[1 + \left(\frac{PR_f}{1.35}\right)^2\right]}} \tag{4}$$

And by expressing Eq. (4) using distance and mass

$$P_{ov} = P_{atm}\frac{808\left[1 + \left(\frac{r_c}{4.5\sqrt[3]{M_e}}\right)^2\right]}{\sqrt{\left[1 + \left(\frac{r_c}{0.048\sqrt[3]{M_e}}\right)^2\right]} \cdot \sqrt{\left[1 + \left(\frac{r_c}{0.32\sqrt[3]{M_e}}\right)^2\right]} \cdot \sqrt{\left[1 + \left(\frac{r_c}{1.35\sqrt[3]{M_e}}\right)^2\right]}} \tag{5}$$

A.N. Skraparlis, K.S. Ntalianis and N. Tsapatsoulis

Table 1
Damage to CI versus overpressure.

| Overpressure	Possible damage
0.4×10^{-1}	Booming sound that may damage glasses
1.5×10^{-1}	Destruction of glasses
4×10^{-1}	Modest damage on the structure of a building
5×10^{-1}–10×10^{-1}	Destruction of windows as well as window-frames
7×10^{-1}	Modest destruction to the structure of homes
10×10^{-1}	Partial destruction of homes
10×10^{-1}–20×10^{-1}	Collapse and warping of corrugated metal panels & Blow away of residential panels made of wood
10×10^{-1}–80×10^{-1}	Injuries, varying from minor to severe lacerations caused by airborne glass and other projectiles
20×10^{-1}	Partial failure of residential walls and roofs
20×10^{-1}–30×10^{-1}	Destruction of walls made by cement that is not reinforced or by concrete blocks
24×10^{-1}–122×10^{-1}	Tympanic membrane perforation for 1 to 90 percent among humans
25×10^{-1}	House brick construction is destroyed by 50 percent
30×10^{-1}	Steel-framed structures warped and detached from their foundation
50×10^{-1}	Destruction of Electricity Power Poles
50×10^{-1}–70×10^{-1}	Homes are almost completely destroyed
70×10^{-1}	Railroad cars are tipped over
90×10^{-1}	Cargo train box cars are destroyed
100×10^{-1}	Buildings are totally destroyed
145×10^{-1}–290×10^{-1}	Human casualties in the range of 1−99 percent, resulting from immediate blast impact

Table 2
$REF(S_i^u)$ for various S_i's.

Chemical formula of S_i	$REF(S_i^u)$
$C_7H_5N_3O_6$ (Trinitrotoluene)	10×10^{-1}
NH_4NO_3	3.2×10^{-1}
$C_6H_{12}N_4O_8$	6×10^{-1}
$C_6H_4(NO_2)2$	6×10^{-1}
$NH_4NO_3 + C_nH_{2n+2}$ (ANFO)	7.4×10^{-1}
$CH_4N_2O_3$	10.5×10^{-1}
$(C_6H_7O_2(ONO_2)_3)n$	11×10^{-1}
$C_6H_3N_3O_7$	11.7×10^{-1}
$C_6H_3N_3O_6$	12×10^{-1}
$C_3H_5N_3O_9$ (Nitroglycerin)	15.4×10^{-1}
$C_3H_6N_6O_6$	16×10^{-1}
$C_8(NO_2)_8$ (Octanitrocubane)	23.8×10^{-1}

Table 4
Classification of drones according to range/endurance.

Drone Range Category	Range/km	Endurance/h
Very Close	<5	0.5−0.75
Close	>5 & <50	1−6
Short	>50 & <150	8−12
Medium	>150 & <650	12−48
Long	>650	>48

Table 5
Characteristic non-military UAVs [18–27].

Name	Max Payload/kg	Max Speed/(km·h⁻¹)	Price/Euro
Griff 800	800	50	240,000
SF-DL-180	100	100	36,000
MH-50	50	36	12,000
JT16L-404QC	22	43	4200
Goliath Quadcopter	18	130	1300
OnyxStar Hydra-12	16	35	4000
YangDa Skywhale Max	15	130	32,000
Freefly Alta X	10	95	17,000
DJI Matrice 300 RTK	2.7	83	13,800
DRL Racer X	1	289	NA
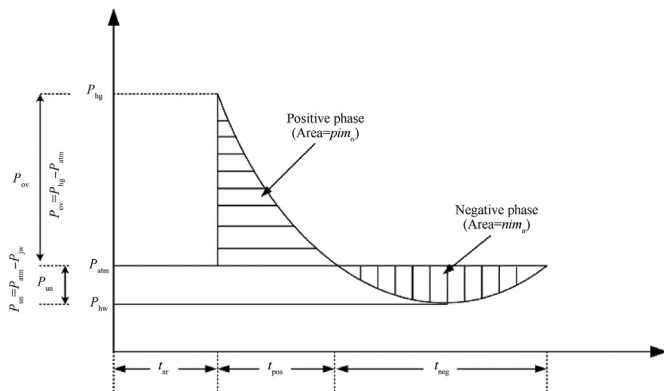
Fig. 1. Wave form of a blast in the open air.

2.4. Non-military UAVs

Various factors can be used to categorize drones. The most common include weight, type of engine, maximum value of flying altitude, autonomy capabilities, role and more. The United States Department of Defense (USDOD), divides drones into five distinct categories [15] (Table 3). Drones can also be classified according to range and endurance (Table 4).

Regarding the degree of autonomy, drones may be human-operated, or have different levels of autonomy, from automated piloting assistance to full autonomy [16,17].

Additionally, Table 5 provides some characteristic non-military drones, available on the market.

As it can be observed and as of January 2024, their maximum payload is between 1 kg and 800 kg, their maximum speed is

Table 3
Classification of drones according to USDOD.

Group	G1	G2	G3	G4	G5
Max take-off weight	<9.1 kg	>9.1 kg & <25 kg	>25 kg & <600 kg	>600 kg	>600 kg
Operating altitude	<370 m	<1.1 km	<5.5 km	<5.5 km	>5.5 km
Speed	<190 km·h⁻¹	<460 km·h⁻¹	<460 km·h⁻¹	Any	Any

A.N. Skraparlis, K.S. Ntalianis and N. Tsapatsoulis

between 35 km/h and 289 km/h and their price is between 1300 Euro and 240,000 Euro.

This paper focuses on relatively low-cost non-military drones, since terrorists can easily find them and turn them into G-B-KDs. It should also be mentioned that military drones need completely different weapons to be neutralized (e.g. *MANPADS*, surface-to-air missiles etc.)

3. Related work

One of the most serious threats that CIs face comes from terrorist drones [28,29]. In the past, several schemes have been proposed to confront this threat. In Ref. [30] multiple agents track and disable a rogue UAV by cooperatively transmitting power from their on-board antennas to jam its communication and sensing receivers. In Ref. [31] the pursuer agent integrates software-defined radio technology to execute rogue drone GPS disruption, while concurrently, autonomous agents collaborate to calculate the location estimate of the pursuer agent. Ref. [32] introduces a narrow beam directors-based Vivaldi antenna, which is designed to cover remotely piloted aircraft system bands. The antenna works as portable anti-drone jammer. In Ref. [33] a Software Defined Radio board is integrated to deploy an RF-based technique for detecting, identifying, and jamming drones. The suggested approach disrupts the wireless link between the drone and ground over the widely utilized frequency of 2.4 GHz. In Ref. [34] a mechanism for detecting drones is suggested. The method utilizes the RF control signal that the drone receives from the remote controller. Subsequently, a high-power signal jams the communication and severs the connection with the controller. In Ref. [35] multiple surveillance drones patrol an area. They identify hostile drones using image processing, surround them and initialize cyber-attacks. In Ref. [36] the DronEnd system incorporates scanning of the RF spectrum, detection of hostile drones based on Angle of Arrival algorithms, and annihilation by RF jamming. Ref. [37] presents a portable system that incorporates software defined radio platforms. The scheme jams malicious drones by generating GPS spoofing signals.

Additionally, there are some neutralization schemes based on directed-energy weapons. In Ref. [38] a Helical Array Antenna releases EMP against commercial drones. Its strength for small ranges is tested, by examining the extent of damage to the drone's electronics. Ref. [39] focuses on laser weapons against drones. The main factors are determined, such as power supply for laser and cooling equipment and system mass. In Ref. [40] machine learning facilitates decision support for warfighters, operating laser weapon systems in intricate tactical scenarios. Wargaming scenarios are simulated and the algorithm forecasts the optimal engagement strategy.

On the other hand, various systems and methods have been proposed to catch or neutralize drones. Ref. [41] presents a drone neutralization system centered around another drone, equipped with a capturing device. The operation depends solely on data recorded by a long-range and a short-range camera. In Ref. [42] a soft-gripper drone is proposed. To avoid aerodynamic disturbances, the gripper utilizes soft actuators, to maintain horizontal orientation and bend when subjected to air pressure. Ref. [43] augments the automation of physical interception operations and optimizes the efficiency of trajectories towards approaching the intruder-drone. Ref. [44] performs autonomous capture of drones, which navigate at various trajectories and speeds. The system also bursts many balloons, distributed randomly across a designated area. Ref. [45] neutralizes drones in GPS-denied. The platform employs a pre-trained model to detect, track, and pursue drones. Ref. [46] examines kinetic energy non-lethal weapons (*KENLW*) to neutralize low, small and slow drones. *KENLW*s launch fast-moving small projectiles. Ref. [47] implements a drone capture device, which uses protective covering to avoid dispersion of the capture net. Following the capture of the target, a pull-off force test is conducted to verify the net's stability. In Ref. [48] neutralization of drones is performed by a swarm of drones that carries a net. Optimal intersection is estimated and flight parameters are described. In Ref. [49] a soft-gripper robot has 3 fingers and touch sensors to accomplish safe capturing of drones. In Ref. [50] a team of drones carries a capture net, which is tensioned by properly adjusting the acceleration of each team-member. In Ref. [51] autonomous interception is achieved by a visual-based servo algorithm. In Ref. [52] a vision-based navigation method seeks and detects intruding drones. Then, the target trajectory is predicted by fusing onboard vision and inertial-measurement resources. Other interesting schemes and related surveys include Refs. [53–60].

Even though very interesting, most of the aforementioned schemes do not consider G-B-KDs. Additionally, they examine
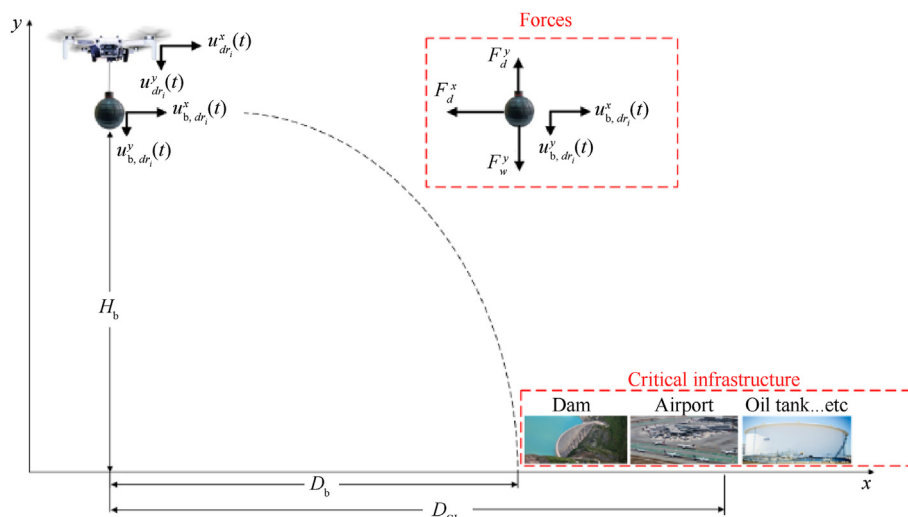

Fig. 2. Illustration of a G-B-KD approaching a CI.

either a net/catching technology or EMP, not both. Furthermore, few approaches estimate the location of interception, while existing algorithms cannot be applied in case of autonomous drones. The proposed scheme considers all these aspects, while its strengths and limitations are revealed through extensive experimentation on simulated data and comparison to the state-of-art.

4. Problem formulation and the proposed scheme

4.1. Problem formulation

In Fig. 2, a G-B-KD approaches a CI (dam, airport, oil tank, etc.). Without loss of generality, the G-B-KD and the bomb are moving on the xy-plane. In order to achieve maximum damage, the G-B-KD should: (a) release its bomb at a specific distance from the CI and (b) crash at the CI.

In order to find the horizontal distance D_b that a bomb will travel when released from a G-B-KD, let us denote by $dr_i, i = 1,2,\cdots,n$, the i-th G-B-KD that carries a bomb and tries to attack a CI. Let us also denote by: (a) $u^x_{dr_i}(t)/u^y_{dr_i}(t)$ the horizontal/vertical velocity of the i-th G-B-KD and (b) $u^x_{b,dr_i}(t)/u^y_{b,dr_i}(t)$ the horizontal/vertical velocity of the bomb of the i-th G-B-KD. Additionally, let us assume that the bomb is released at $t = 0$ and at height H_b. D_{CI} is the horizontal distance of the bomb from CI. If $D_b < D_{CI}$, then the CI is not directly hit. However, its safety also depends on the blast pressure (Eq. (5) and Table 1).

In order to establish a real-world model of the trajectory of the bomb, the drag is taken into account. According to Ref. [61] up to velocities of about 877 km/h (800 ft/s) the simple square drag law holds for solid shell-like bodies.

Fig. 2 illustrates the forces exerted on the released bomb. F^x_d/ F^y_d is the air resistance at the x/y axis, respectively, while F^y_w is the gravitational force. When the bomb is released from the G-B-KD, its trajectory will vary in curvature. Then, two-dimensional motion can be approximated by two one-dimensional motions, along the x and y-axis, since no analytic solution is possible for two-dimensional motions [62]. Additionally, the bomb is considered having a sphere's shape.

Initially the vertical motion is considered. In this case, F^y_d can be expressed by [62]

$$F^y_d = \frac{1}{2}\rho_a C_d A_b \left(ur^y_{b,dr_i}\right)^2 \tag{6}$$

where ρ_a is the density of the air, C_d is the drag coefficient, A_b is the effective cross-sectional area of the bomb and ur^y_{b,dr_i} is the relative velocity between the bomb and the air.

Then in the y direction we have

$$F^y_b = F^y_w - F^y_d \tag{7}$$

where the total force F^y_b can be expressed as

$$F^y_b = m_b\gamma^y_b \tag{8}$$

m_b is the mass and γ^y_b is the acceleration of the bomb.

Additionally

$$F^y_w = m_b g \tag{9}$$

where g is the gravity.

Furthermore, when $F^y_w = F^y_d$ then the bomb reaches terminal velocity (ur^y_{term}). In this case

$$m_b g = \frac{1}{2}\rho_a C_d A_b \left(ur^y_{term}\right)^2 => ur^y_{term} = \sqrt{\frac{2m_b g}{\rho_a C_d A_b}} \tag{10}$$

Then Eq. (7) becomes

$$m_b\gamma^y_b = m_b g - \frac{1}{2}\rho_a C_d A_b \left(ur^y_{b,dr_i}\right)^2 => \gamma^y_b = g\left(1 - \frac{\left(ur^y_{b,dr_i}\right)^2}{\left(ur^y_{term}\right)^2}\right) \tag{11}$$

To get the velocity-time formula, acceleration is integrated

$$\frac{d\left(ur^y_{b,dr_i}\right)}{dt} = g\left(1 - \frac{\left(ur^y_{b,dr_i}\right)^2}{\left(ur^y_{term}\right)^2}\right) => \frac{d\left(ur^y_{b,dr_i}\right)}{\left(1 - \frac{\left(ur^y_{b,dr_i}\right)^2}{\left(ur^y_{term}\right)^2}\right)} = gdt => \int \frac{d\left(ur^y_{b,dr_i}\right)}{\left(1 - \frac{\left(ur^y_{b,dr_i}\right)^2}{\left(ur^y_{term}\right)^2}\right)} = g\int dt \tag{12}$$

By substituting

$$\frac{ur^y_{b,dr_i}}{ur^y_{term}} = w => dw = \frac{d\left(ur^y_{b,dr_i}\right)}{ur^y_{term}} \tag{13}$$

$$ur^y_{term}\int \frac{\frac{d\left(ur^y_{b,dr_i}\right)}{ur^y_{term}}}{\left(1 - \frac{\left(ur^y_{b,dr_i}\right)^2}{\left(ur^y_{term}\right)^2}\right)} = g\int dt => ur^y_{term}\int \frac{dw}{1 - w^2} = g\int dt \tag{14}$$

Since

$$\int \frac{dw}{1 - w^2} = \text{arctanh}\,(w) \tag{15}$$

Eq. (14) becomes

$$\text{arctanh}\,\frac{ur^y_{b,dr_i}}{ur^y_{term}} = \frac{gt}{ur^y_{term}} + C \tag{16}$$

Since

A.N. Skraparlis, K.S. Ntalianis and N. Tsapatsoulis

$$\operatorname{arctanh}(y) = x => \tanh(x) = y \tag{17}$$

Eq. (16) becomes

$$ur^{y}_{b,dr_i}(t) = ur^{y}_{term} \tanh\left(\frac{gt}{ur^{y}_{term}} + C\right) \tag{18}$$

In our problem

$$ur^{y}_{b,dr_i}(0) = 0 => C = 0 \tag{19}$$

As a result, Eq. (18) becomes

$$ur^{y}_{b,dr_i}(t) = ur^{y}_{term} \tanh\left(\frac{gt}{ur^{y}_{term}}\right) \tag{20}$$

In order to calculate the position of the bomb at the y-axis as a function of time

$$y(t) = \int d\left(ur^{y}_{b,dr_i}\right) = ur^{y}_{term} \int \tanh\left(\frac{gt}{ur^{y}_{term}}\right) dt \tag{21}$$

And by making the following substitution

$$\gamma^x_b = \frac{d\left(ur^x_{b,dr_i}\right)}{dt} = -\frac{\rho_a C_d A_b}{2m_b}\left(ur^x_{b,dr_i}\right)^2 => \frac{d\left(ur^x_{b,dr_i}\right)}{\left(ur^x_{b,dr_i}\right)^2} = -\frac{\rho_a C_d A_b}{2m_b}dt => \int \frac{1}{\left(ur^x_{b,dr_i}\right)^2}d\left(ur^x_{b,dr_i}\right) = -\frac{\rho_a C_d A_b}{2m_b}\int dt => -\frac{1}{ur^x_{b,dr_i}} =$$

$$-\frac{\rho_a C_d A_b}{2m_b}t + C$$

$$\tag{32}$$

$$\frac{gt}{ur^{y}_{term}} = z => \frac{ur^{y}_{term}}{g}dz = dt \tag{22}$$

Eq. (21) becomes

$$ur^{y}_{term} \int \tanh(z) \frac{ur^{y}_{term}}{g}dz = \frac{(ur^{y}_{term})^2}{g}\int \tanh(z)dz \tag{23}$$

And since

$$\int \tanh(z)dz = \ln(\cosh(z)) + C \tag{24}$$

Eq. (23) becomes

$$y(t) = \frac{(ur^{y}_{term})^2}{g}\ln\left(\cosh\left(\frac{gt}{ur^{y}_{term}}\right)\right) + C \tag{25}$$

In our problem:

$$y(0) = 0 => C = 0 \tag{26}$$

As a result, Eq. (25) becomes

$$y(t) = \frac{(ur^{y}_{term})^2}{g}\ln\left(\cosh\left(\frac{gt}{ur^{y}_{term}}\right)\right) \tag{27}$$

Let us now consider the horizontal motion of the bomb

$$F^x_d = \frac{1}{2}\rho_a C_d A_b\left(ur^x_{b,dr_i}\right)^2 \tag{28}$$

where ur^x_{b,dr_i} is the relative velocity between the bomb and the air. Then, in the x direction

$$F^x_b = -F^x_d \tag{29}$$

In this case

$$m_b\gamma^x_b = -\frac{1}{2}\rho_a C_d A_b\left(ur^x_{b,dr_i}\right)^2 \tag{30}$$

or

$$\gamma^x_b = -\frac{\rho_a C_d A_b}{2m_b}\left(ur^x_{b,dr_i}\right)^2 \tag{31}$$

To get the velocity-time formula, acceleration is integrated

where C is a constant. Since $ur^x_{b,dr_i}(0) = u^x_{dr_i}(0)$, from Eq. (32) we have

$$C = -\frac{1}{u^x_{dr_i}(0)} \tag{33}$$

Then Eq. (32) becomes

$$\frac{1}{ur^x_{b,dr_i}} = \frac{\rho_a C_d A_b}{2m_b}t + \frac{1}{u^x_{dr_i}(0)} => \frac{1}{ur^x_{b,dr_i}}$$

$$= \frac{1}{u^x_{dr_i}(0)}\left(1 + \frac{\rho_a C_d A_b u^x_{dr_i}(0)}{2m_b}t\right) \tag{34}$$

And by denoting

$$\tau = \frac{2m_b}{\rho_a C_d A_b u^x_{dr_i}(0)} \tag{35}$$

Eq. (34) becomes

$$\frac{1}{ur^x_{b,dr_i}} = \frac{1}{u^x_{dr_i}(0)}\left(1 + \frac{t}{\tau}\right) => ur^x_{b,dr_i}(t) = \frac{u^x_{dr_i}(0)}{1 + \frac{t}{\tau}} \tag{36}$$

Then, the position of the bomb as a function of time is calculated

$$\frac{\mathrm{d}x}{\mathrm{d}t} = ur_{b,dr_i}^{\chi}(t) = \frac{u_{dr_i}^{x}(0)}{1 + \frac{t}{\tau}} => \mathrm{d}x = \frac{u_{dr_i}^{x}(0)}{1 + \frac{t}{\tau}} \mathrm{d}t => \int \mathrm{d}x$$

$$= \int \frac{u_{dr_i}^{x}(0)}{1 + \frac{t}{\tau}} \mathrm{d}t \tag{37}$$

And since

$$\int \frac{1}{1 + ax} \mathrm{d}x = \frac{1}{a} \ln(1 + ax) + C \tag{38}$$

Eq. (37) becomes

$$x(t) = u_{dr_i}^{x}(0)\tau \ln\left(1 + \frac{t}{\tau}\right) + C \tag{39}$$

In our problem

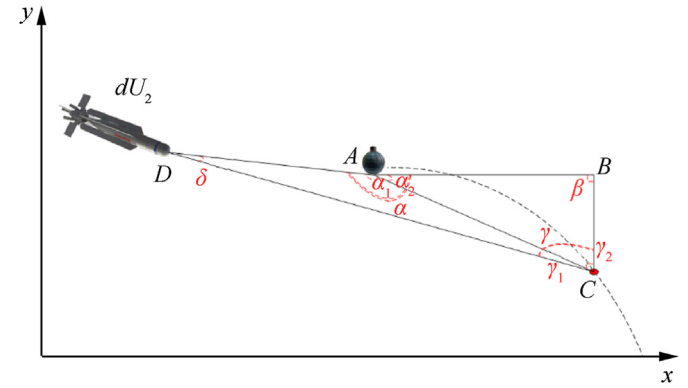$$x(0) = 0 => C = 0 \tag{40}$$

As a result, Eq. (39) becomes

Fig. 4. dU_2 moving towards the location of interception C (engagement with bomb).

$$x(t) = u_{dr_i}^{x}(0)\tau \ln\left(1 + \frac{t}{\tau}\right) \tag{41}$$
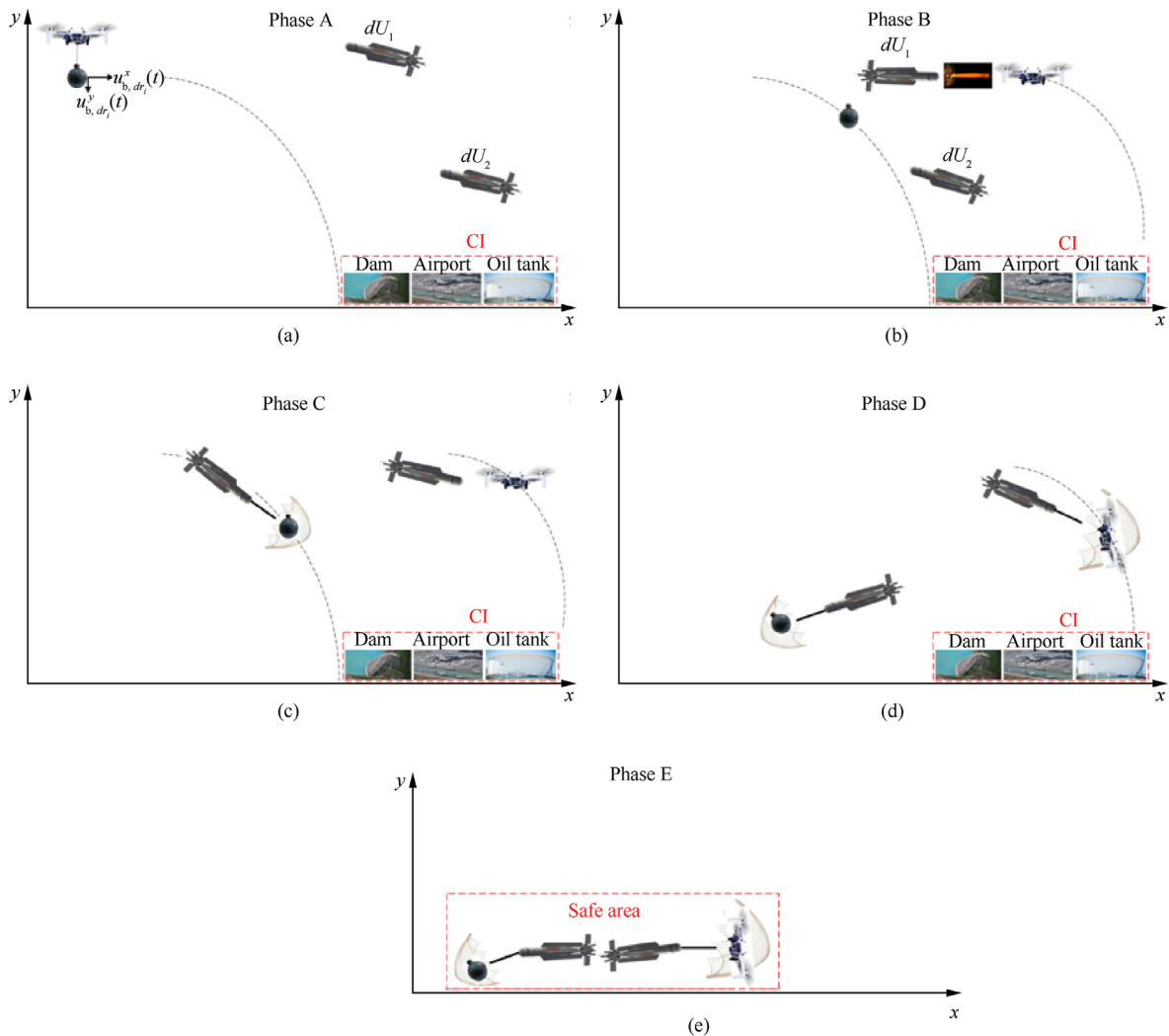

(a)

(b)

(c)

(d)

(e)

Fig. 3. (a) G-B-KD releasing a bomb. dU_1 and dU_2 on their way to intercept the threats; (b) dU_1 releasing EMP. dU_2 moving towards the location of interception with the bomb; (c) dU_2 releasing the net and capturing the bomb. dU_1 moving towards the location of interception with the G-B-KD; (d) dU_1 releasing the net and capturing the G-B-KD. dU_2 moving towards the safe area; (e) dU_1 and dU_2 at the safe area.

4.2. The proposed scheme based on a couple of DDs

Let us assume that the G-B-KD is able to detect the DDs (e.g. by proximity sensors) and, in this case, it is programmed to release the bomb before the DDs arrive. Let us denote by dU_1 and dU_2 the two specially equipped DDs, where dU_1 neutralizes and captures the G-B-KD, while dU_2 captures the bomb. dU_1 and dU_2 are equipped with a net-gun and a processing unit which runs the proposed Algorithm 1, while dU_1 is also equipped with an EMP weapon. Here, the following should be mentioned: (a) there are drones such as Raytheon Coyote Block 3 [63], which use EMP and drones that use net-guns [43,47,48,50] (b) to the best of the authors' knowledge there are not any drones that incorporate both weapons and utilize trajectory estimation (Eqs. (27) and (41)), so that to calculate the optimal locations of interception.

Additionally, let us assume that the maximum speeds that dU_1 and dU_2 can reach are $u_{\max,dU_1}$ and $u_{\max,dU_2}$ respectively. Then, the following conditions are required

$$u_{\max,dU_1} \gg u_{dr_i}^y(t) \ \& \ u_{\max,dU_1} \gg u_{dr_i}^x(t), \ \forall t \tag{42}$$

$$u_{\max,dU_2} \gg ur_{\text{term}}^y \tag{43}$$

According to Eq. (42), dU_1 moves much faster than dr_i, $i = 1, 2, \cdots, n$, and according to Eq. (43), dU_2 can reach speeds that highly surpass the terminal velocity of the bomb. Both conditions can be satisfied by different drones (e.g. Raytheon Coyote Block 2, reaches 555 km/h [64]).

Fig. 3 illustrates the five phases of the proposed framework, which may not necessarily be sequential. Additionally, phases are not in chronological order, e.g., Phase C may be completed before Phase B etc.

The locations of interception (with the bomb/G-B-KD) are the spatial points where dU_1 intercepts the free-fall G-B-KD, (after Phase B) and dU_2 intercepts the bomb. These locations can be estimated for all arrangements of G-B-KD, DDs and the bomb. An example is provided in Fig. 4. In particular, let us suppose that the interception location of dU_2 and the bomb is C, where C is reached by both the bomb and dU_2 at $t = t_{e,b}$. Angles α and γ (Fig. 4) can be expressed as

$$\alpha = \alpha_1 + \alpha_2 \tag{44}$$

$$\gamma = \gamma_1 + \gamma_2 \tag{45}$$

Then

$$CD^2 = AC^2 + AD^2 - 2AC \cdot AD \cdot \cos \alpha_1 \tag{46}$$

and according to Eq. (44) α.

$$\cos \alpha_1 = \cos \alpha \cdot \cos \alpha_2 + \sin \alpha \cdot \sin \alpha_2 \tag{47}$$

while

$$\sin \alpha_2 = \frac{BC}{AC} \tag{48}$$

$$\cos \alpha_2 = \frac{AB}{AC} \tag{49}$$

and

$$AC^2 = AB^2 + BC^2 \tag{50}$$

Additionally

$$AB = x(t_{e,b}) = u_{dr_i}^x(0)\tau \ln\left(1 + \frac{t_{e,b}}{\tau}\right) \tag{51}$$

$$BC = y(t_{e,b}) = \frac{(ur_{\text{term}}^y)^2}{g} \ln\left(\cosh\left(\frac{gt_{e,b}}{ur_{\text{term}}^y}\right)\right) \tag{52}$$

$$CD = u_{\max,dU_2} \cdot t_{e,b} \tag{53}$$

Then Eq. (45) becomes

$$u_{\max,dU_2}^2 \cdot t_{e,b}^2 - \left(x^2(t_{e,b}) + y^2(t_{e,b})\right) - AD^2$$
$$+ 2\sqrt{x^2(t_{e,b}) + y^2(t_{e,b})} \cdot AD(\cos \alpha \cdot \cos \alpha_2 + \sin \alpha \cdot \sin \alpha_2)$$
$$= 0 \tag{54}$$

In Eq. (54) α and AD can be efficiently approximated, e.g. by using multilateral radar triangulation (MRT) [65] to geolocate the target. As a result, even though it is difficult to analytically solve Eq. (54) for $t_{e,b}$, an arithmetic solution is straightforward.

Then the innovative Algorithm 1 intercepts the G-B-KD. Algorithm 1 has two parts: initialization and interception. During initialization, dU_1 and dU_2 receive from the MRT, the speed and location of the G-B-KD and start moving towards it. Interception assumes that the G-B-KD releases the bomb. In this case and in parallel: (a) dU_2 receives from the MRT parameters α and AD, estimates the trajectory of the bomb as well as $t_{e,b}$, moves towards the interception location C, captures the bomb and lands at a safe area, (b) dU_1 moves towards the G-B-KD and when it is close enough it releases the EMP. Then it receives from the MRT parameters α and AD, estimates the trajectory of the bomb as well as $t_{e,b}$, moves towards the interception location C, captures the G-B-KD and lands at a safe area.

Here, the differences between the proposed method and Proportional Navigation (PN) are also emphasized, since PN is a guidance law that is predominantly used for homing missiles and aerospace interceptors. In PN even when the target does not maneuver, the pursuer follows a curved trajectory as it continuously adjusts its velocity to maintain the pursuit and minimize the Line-of-Sight (LOS). In contrast to PN, the proposed method follows a straight line (DC in Fig. 4). The straight line is the minimum distance (leading to the minimum interception time) between pursuer and target. On the other hand, the curved path provided by PN is not the minimum distance between pursuer and target and it does not lead to the minimum interception time. For small DA (Fig. 4) in the range of 5−10 m, interception times from PN and the proposed method are similar, but as DA increases the difference between interception times also increases. Here it should be mentioned that in the proposed scheme, DA depends on the power of the EMP weapon. In any case, the interception time of the proposed scheme is always less than the interception time of PN. Additionally, PN's results depend on a positive navigation constant, usually denoted by N_1. Different values of N_1 provide different interception times. On the contrary, the interception time of the proposed scheme does not depend on the selection of any parameters. Finally, the

A.N. Skraparlis, K.S. Ntalianis and N. Tsapatsoulis

Algorithm 1: Generic Interception of G-B-KD

// ######## **INITIALIZATION** ########
if (MRT.detect > 0**)** // G-B-KD detected by MRT (multilateral radar triangulation) near *CI*
then
  {
  dU_1.MRT_receive.location -> $(x_d(t), y_d(t))$ &
  & dU_2.MRT_receive.location -> $(x_d(t), y_d(t))$ // dU_1 and dU_2 continuously
   receive estimated location of G-B-KD, where $y_d(t) = H_b$
  dU_1.MRT_receive.speed -> $(u_{dr_i}^y(t), u_{dr_i}^x(t))$ &
  & dU_2.MRT_receive.speed -> $(u_{dr_i}^y(t), u_{dr_i}^x(t))$ // dU_1 and dU_2
  continuously receive estimated speed of G-B-KD
  dU_1.move.to $(x_d(t), y_d(t))$ = true &
  & dU_2.move.to$(x_d(t), y_d(t))$ = true // dU_1 and dU_2 go towards the target
  }
       // ######## **BOMB &** G-B-KD **INTERCEPTION** ########
if {G-B-KD.*release_bomb* == *"true"*} // G-B-KD releases bomb
then do in parallel
{
  { // running on dU_2
  dU_2.MRT_receive.parameters -> (a_b, AD_b) // dU_2 receives a and AD of
  the bomb (a_b, AD_b) from MRT (Fig. 4)
  dU_2.estimate -> $(x(t), y(t))$ // dU_2 estimates trajectory of the bomb using
  Eq. (27) and Eq. (41)
  dU_2.calculate -> $t_{e,b}$ // dU_2 calculates time to intercept bomb using Eq.
  (54)

  dU_2.move.to -> C // dU_2 goes to the bomb interception location (Fig. 4)
  dU_2.use.netgun = true // dU_2 releases net and captures bomb
  dU_2.land.safe = true // dU_2 & captured bomb land at safe area
 } // end running on dU_2
  {// running on dU_1
 dU_1.MRT_receive.location -> $(x_d(t), y_d(t))$ // dU_1 continuously receives
estimated location of G-B-KD
dU_1.move.to $(x_d(t), y_d(t))$ = true // dU_1 goes towards the G-B-KD
dU_1.MRT_receive.parameters -> (AD_d) // dU_1 continuously receives AD
of the G-B-KD (AD_d) from MRT (Fig. 4)
  if $(AD_d < EMP\_thresh)$ // dU_1 is close enough to G-B-KD
  then{
     dU_1.use.EMP = true // dU_1 releases EMP
     dU_1.MRT_receive.parameters -> (a_d, AD_d) // dU_1 receives a and
     AD of the G-B-KD (a_d, AD_d) from MRT (Fig. 4)
     dU_1.estimate -> $(x(t), y(t))$ // dU_1 estimates trajectory of the
     G-B-KD using Eq. (27) and Eq. (41)
     dU_1.calculate -> $t_{e,b}$ // dU_1 calculates time to intercept G-B-KD
     using Eq. (54)
     dU_1.move.to -> C // dU_1 goes to the G-B-KD interception location
     (Fig. 4)
     dU_1.use.netgun = true // dU_1 releases net and captures G-B-KD
     dU_1.land.safe = true // dU_1 & captured G-B-KD land at safe area
   }
  } // end running on dU_1
} **end do in parallel**

A.N. Skraparlis, K.S. Ntalianis and N. Tsapatsoulis

computational complexity of PN is higher compared to the proposed scheme. In particular, in case of PN, the pursuer has to: (a) continuously estimate the LOS angular rate and the rate of change of the distance from the pursuer to the target and (b) adjust its path in order to intercept the target. On the contrary, Eq. (54) of the paper has to be arithmetically solved only once.

5. Experimental results

Experimental simulations and comparisons were carried out using a PC with Intel(R) Core i7-12700 CPU @ 3.60 GHz and 16 GB DDR4 RAM. R 4.3.1 was also incorporated.

Initially, a worst-case scenario is analyzed for ANFO, TNT and Octanitrocubane (Table 2). It is assumed that all G-B-KDs are rigged with ANFO, TNT or Octanitrocubane and carry one releasable bomb of the same substance. Here it should be mentioned that: (a) similar calculations are available for all substances of Table 2 and (b) based on each explosive's cost, it is likely that terrorists will use ANFO (~400 Euro/ton) [66], or TNT (~2000 Euro/ton) [67].

Octanitrocubane is unlikely to be used, since its base (dimethyl cubane-1,4-dicarboxylate) has a cost of about 36,000 Euro/kg [68], which is much higher than the cost of buying a non-military UAV or the cost of buying other weapons. According to the worst-case scenario, all G-B-KDs carry the maximum load (bomb + rigged explosives), as terrorists seek to maximize the overall impact of an attack. The maximum load for different non-military UAVs is provided in Table 5, while results are provided for six different masses: $M_1 = 100$ kg, $M_2 = 50$ kg, $M_3 = 25$ kg, $M_4 = 10$ kg, $M_5 = 5$ kg, and $M_6 = 1$ kg. Griff 800 (Table 5) has a maximum payload of 800 kg. This threat cannot be confronted by the proposed scheme, since it is extremely difficult to capture with a net, carry and land such a huge payload and further research should be carried out.

Fig. 5(a) (ANFO), 5(b) (TNT) and 5(c) (OCTANITROCUBANE) show overpressure (log10) versus distance (m) from a CI, for the six different masses (M_1-M_6) and for the following distances: 0.01 m (point-blank), 1 m, 2 m, 5 m, 10 m, 20 m, 40 m, 50 m, 100 m, 150 m, 200 m, 250 m, 300 m, 350 m, 400 m, 450 m, and 500 m. As it can be observed: (a) the maximum overpressure is 11,867.51 psi for M_1 of Octanitrocubane at 0.01 m, (b) a bomb/G-B-KD explosion is very dangerous (psi >1 − Table 1) for distances more than 50 and less than 100 m for 100 kg. In this case ANFO provides 1.16 psi (50 m) and 0.53 psi (100 m), TNT provides 1.31 psi (50 m) and 0.59 psi (100 m) and Octanitrocubane provides 1.95 psi (50 m) and 0.81 psi (100 m) and (c) the explosion is dangerous even for M_6 and for distances 10 m−20 m. In this case ANFO provides 1.27 psi (10 m) and 0.57 psi (20 m), TNT provides 1.45 psi (10 m) and 0.64 psi (20 m) and Octanitrocubane provides 2.17 psi (10 m) and 0.88 psi (20 m).

For the next experiments and without loss of generality, it is assumed that the bomb is spherical ($C_d = 0.47$) and it follows the ground burst condition, while the G-B-KD may follow either the ground or the air burst condition, before stricken by the EMP. After stricken by the EMP it can follow only the ground burst condition. Additionally, $\rho_a = 1.204$ kg/m^3, $g = 9.81$ m/s^2, while

$$A_b = \pi \cdot R^2 \qquad (55)$$

where R is the radius of the sphere. Since six different bomb masses are considered, it is assumed that each sphere has a different radius, leading to the following six radius-mass couples: (0.05 m, M_6), (0.1 m, M_5), (0.13 m, M_4), (0.20 m, M_3), (0.25 m, M_2) and (0.3 m, M_1).

Furthermore, according to Table 5, the M_6 mass can move at a top speed of 289 km/h (80.28 m/s), the M_5 and M_4 masses can move at 130 km/h (36.11 m/s), while the M_3, M_2, and M_1 masses can move at 100 km/h (27.28 m/s). Then, the bombs' trajectories for
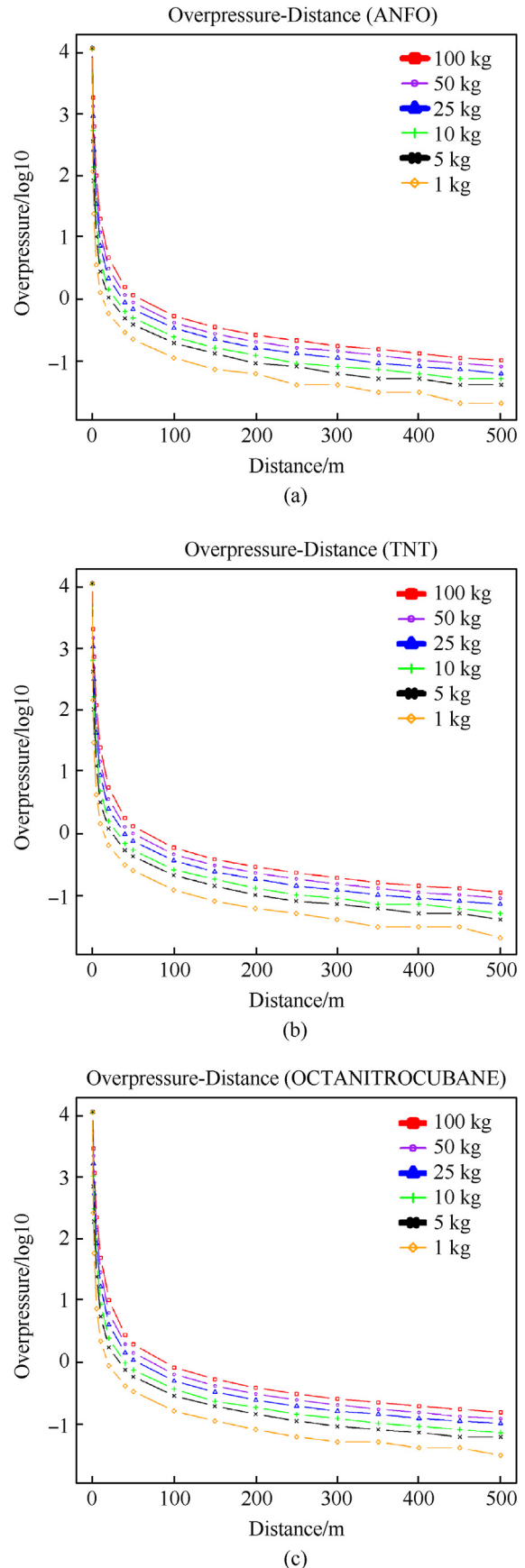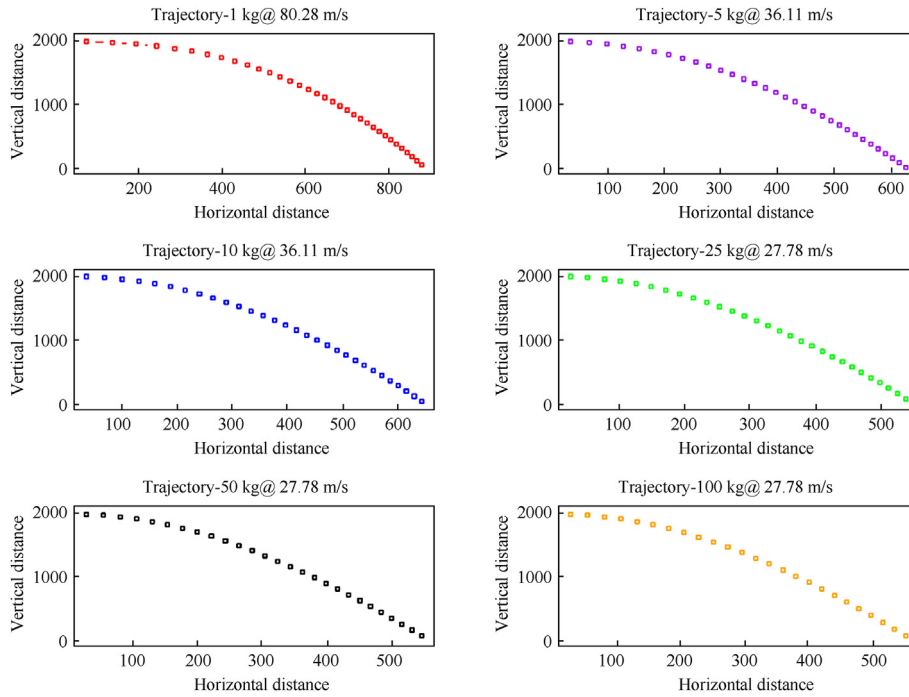

(a)

(b)

(c)

Fig. 5. Overpressure (log10) versus distance (m) for six different masses (M_1−M_6) and seventeen distances (0.01−500 m): (a) ANFO; (b) TNT; (c) Octanitrocubane.

A.N. Skraparlis, K.S. Ntalianis and N. Tsapatsoulis

Fig. 6. Bomb trajectory for six different masses (M_1–M_6) with $H_b = 2000$ m: M_6 at 80.28 m/s (289 km/h), M_5 at 36.11 m/s (130 km/h), M_4 at 36.11 m/s (130 km/h), M_3 at 27.28 m/s (100 km/h), M_2 at 27.28 m/s (100 km/h) and M_1 at 27.28 m/s (100 km/h).

$H_b = 2,000$ m are illustrated in Fig. 6. As it can be observed, M_6 travels horizontally for about 880 m until it reaches the ground. The values for M_5, M_4, M_3, M_2, and M_1 are about 628 m, 643 m, 537 m, 546 m, and 552 m respectively. The times of flight are also different. M_6 reaches the ground at about 34 s. The values for the other five masses are about 32 s, 30 s, 29 s, 27 s, and 25 s respectively. If the bombs are released from $H_b = 50$ m, then, all of them reach the ground in less than 3 s.

According to the above results (Figs. 5 and 6), the couple of the

Fig. 7. Minimum take-off distance for six different masses (M_1–M_6) with $H_b = 2000$ m: (a) M_6 at 80.28 m/s (289 km/h); (b) M_5 at 36.11 m/s (130 km/h); (c) M_4 at 36.11 m/s (130 km/h); (d) M_3 at 27.28 m/s (100 km/h); (e) M_2 at 27.28 m/s (100 km/h) and (f) M_1 at 27.28 m/s (100 km/h).

DDs should take off in time in order to successfully deal with the various threats. It is assumed that the DDs take off from the ground, matching the arrangements of Figs. 3 and 4. Additionally, due to the proposed modifications, it is assumed that the DDs could reach a top speed of 444 km/h, at a 5 g sustained acceleration (e.g. 20% less than the original Raytheon Coyote Block 2) [64,69].

Thus, they reach top speed in 9.05 s, covering a distance of 2008.66 m. After this distance, the DDs fly at top speed. Furthermore, it is assumed that $H_b = 2000$ m and the G-B-KD flies at its top speed to reach a point, where it can release the bomb (release-point). The release-point is different for the different masses and it depends on two factors: (a) the trajectory of the bomb (covered horizontal distance − Fig. 6) and (b) the blast overpressure (Fig. 5). For example, in case of M_6 at 80.28 m/s the horizontal distance is 880 m while the blast overpressure falls under one (psi<1) for distances over 20 m. In this case, the minimum horizontal distance to intercept the G-B-KD is 900 m (880 m trajectory +20 m blast). Since $H_b = 2000$ m, according to the Pythagorean theorem and solving for the hypotenuse, the Euclidean distance of the release-point to intercept the G-B-KD is 2193.17 m. Similar calculations were performed for M_5 at 36.11 m/s, M_4 at 36.11 m/s, M_3 at 27.28 m/s, M_2 at 27.28 m/s, and M_1 at 27.28 m/s. Of course, the G-B-KD can release the bomb earlier, however, in this case the bomb will not damage the CI, but it may harm people and damage their properties (houses, cars etc.). In this paper it is assumed that the G-B-KD aims at damaging CIs, thus it tries to reach the release-point. However, if the mission of the G-B-KD is threatened by the DDs, it is assumed that it is programmed to release the bomb as close to the release-point as possible. Having estimated the release-point of the bomb and by knowing the top speed of the G-B-KD, the minimum distance, at which the DDs should take off can be estimated. For example, in case of M_6 at 80.28 m/s, the DD reaches top speed at 9.05 s, having covered a distance of 2008.66 m. In order to reach the release-point (2193.17 m) it needs 1.5 more second and from take-off 10.55 s in total (9.05 s + 1.5 s). On the other hand, the G-B-KD covers a distance of 846.95 m in 10.55 s. It is assumed that the G-B-
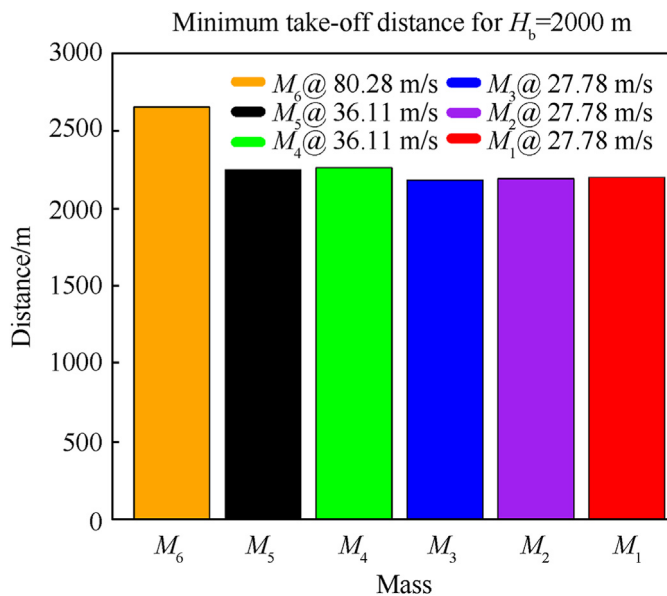
KD moves horizontally, since its flying height is crucial to succeed to its mission. As a result, the DDs should take-off when the horizontal distance of the G-B-KD is 1746.95 m (900 m + 846.95 m). Solving again for the hypotenuse, the minimum distance of the G-B-KD from the CI at which the DDs should take-off is calculated. In the examined case, the distance is 2.655,33 m.

Fig. 7 provides the minimum take-off distances for all six masses (M_1-M_6) and for their respective speeds. As it can be observed the six couples of mass-take-off distance are: $(M_1$, 2199 m), $(M_2$, 2191.95 m), $(M_3$, 2183.73 m), $(M_4$, 2259.53 m), $(M_5$, 2246.93 m), and $(M_6$, 2655.33 m). Here it should be mentioned that the distance for M_1, M_2, and M_3 at 27.78 m/s slightly decreases, due to the decrease of the mass, since τ increases with mass (Eq. (41) and (35)). Similar observations apply to M_4 and M_5 at 36.11 m/s.

5.1. Comparison to state-of-art

In this subsection, the proposed approach is compared to the following state-of-art approaches: (a) LM: loitering munition (exploding UAV) [70], (b) DUNnE: DD with net, without EMP [43,47,48,50], (c) DUNE: DD with net and EMP. It is also assumed that the aforementioned compared DDs do not include the proposed innovative point-of-interception computational method, but use the very common Go-onto-target (GOT) guidance system [71] to follow the target, during the phase of free fall with air resistance. More specifically, a semi-active radar homing (SARH) is assumed to be adopted by the three compared schemes. The SARH combines a passive radar receiver on the DD with a separate targeting radar that marks the target. SARH is the most common guidance solution for ground- and air-launched anti-aircraft systems [72].

Before providing experimental results, the following points are made: (a) in all approaches it is assumed that the DDs fly at top speed to approach the target, (b) in all approaches it is assumed that the DDs are not on a collision course with the targets, but chase the targets by following their tails, (c) LM explodes when its distance from the target is less than 5 m, (d) DUNnE approaches the target to less than 5 m and releases the net after keeping this distance for about t_{r1} s (reducing probability to miss the target), where t_{r1} depends on the mass of the target, (e) DUNE approaches the G-B-KD to less than 5 m and releases the EMP, causing the G-B-KD to start its free fall with air resistance. Then DUNE approaches the target to less than 5 m and releases the net, after keeping this distance for about t_{r2} s, (f) in this paper $t_{r1}>t_{r2}$, since DUNnE does not use EMP to interrupt the autonomous flight of the target. As a result, the G-B-KD may change its flight characteristics (speed, acceleration, direction etc.) at any time. Thus, DUNnE waits for a little more before releasing the net, to increase the success of capturing the target.

In the following experiments t_{r1}/t_{r2} is set to 3/2 $\pm$10% s for M_1, M_2 and M_3 and to 2/1 $\pm$10% s for M_4, M_5 and M_6. The $\pm$10% provides some flexibility to the estimations, in order to cover most cases. Threshold t_{r2} is also used by the proposed scheme. Fig. 8 provides the time to neutralize the target, for all six masses (M_1-M_6) and for initial distances from 50 m to 800 m.

The initial distance $(AD - Fig. 4)$ is the Euclidian distance between dU_2 and the mass at $t = 0$ (bomb released at $t = 0$ from height H_b). In Fig. 8, the scale of x-axis (time) is 1/10 of a second. As it can be observed, LM provides better results than DUNnE and DUNE. Compared to the proposed scheme: (a) in case of M_6, LM performs better only for an initial distance of 50 m. For more than 50 m the proposed scheme provides better performance, (b) in cases of M_5 and M_4 LM performs better for initial distances up to 250 m. For more than 250 m the proposed scheme provides better performance, (c) in case of M_3, LM performs better for initial distances up
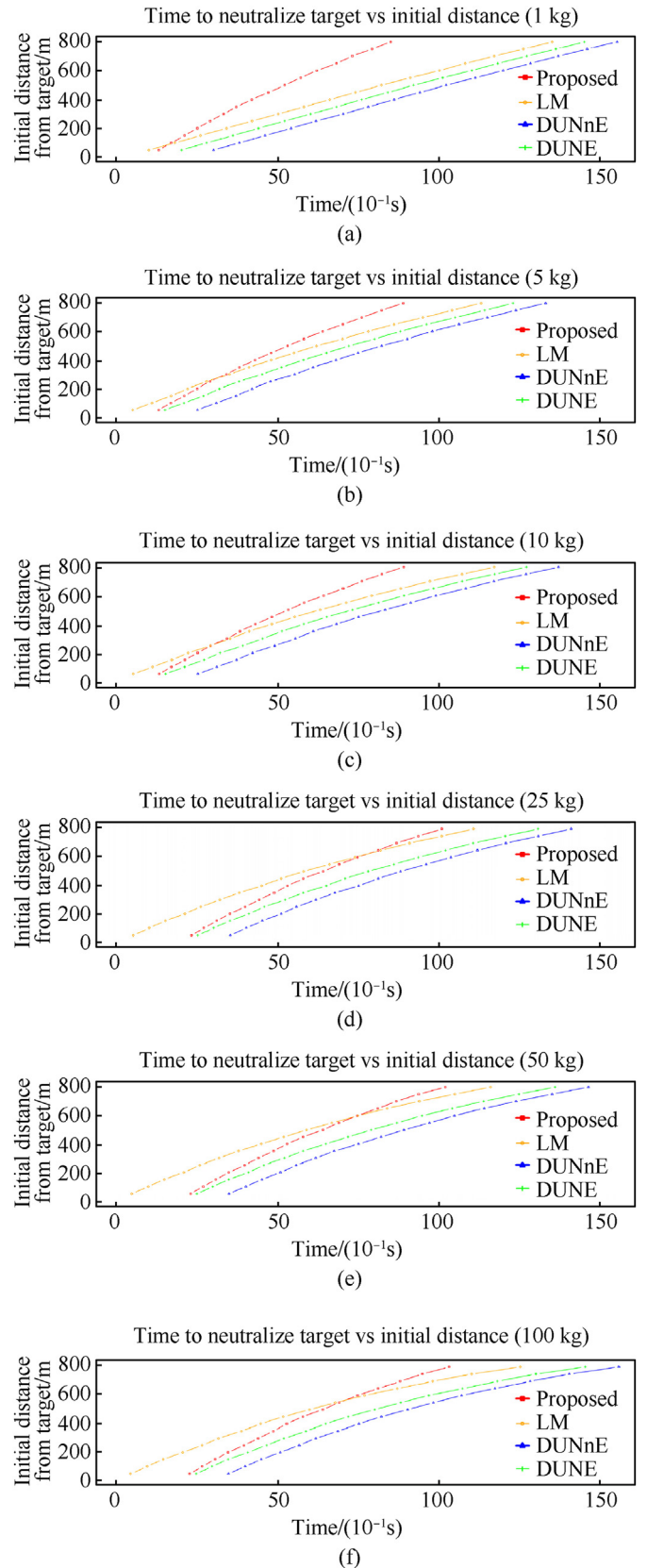

Fig. 8. Time to neutralize target for different initial distances (50 m–800 m): (a) M_6 at 80.28 m/s, (b) M_5 at 36.11 m/s, (c) M_4 at 36.11 m/s, (d) M_3 at 27.28 m/s, (e) M_2 at 27.28 m/s, and (f) M_1 at 27.28 m/s.
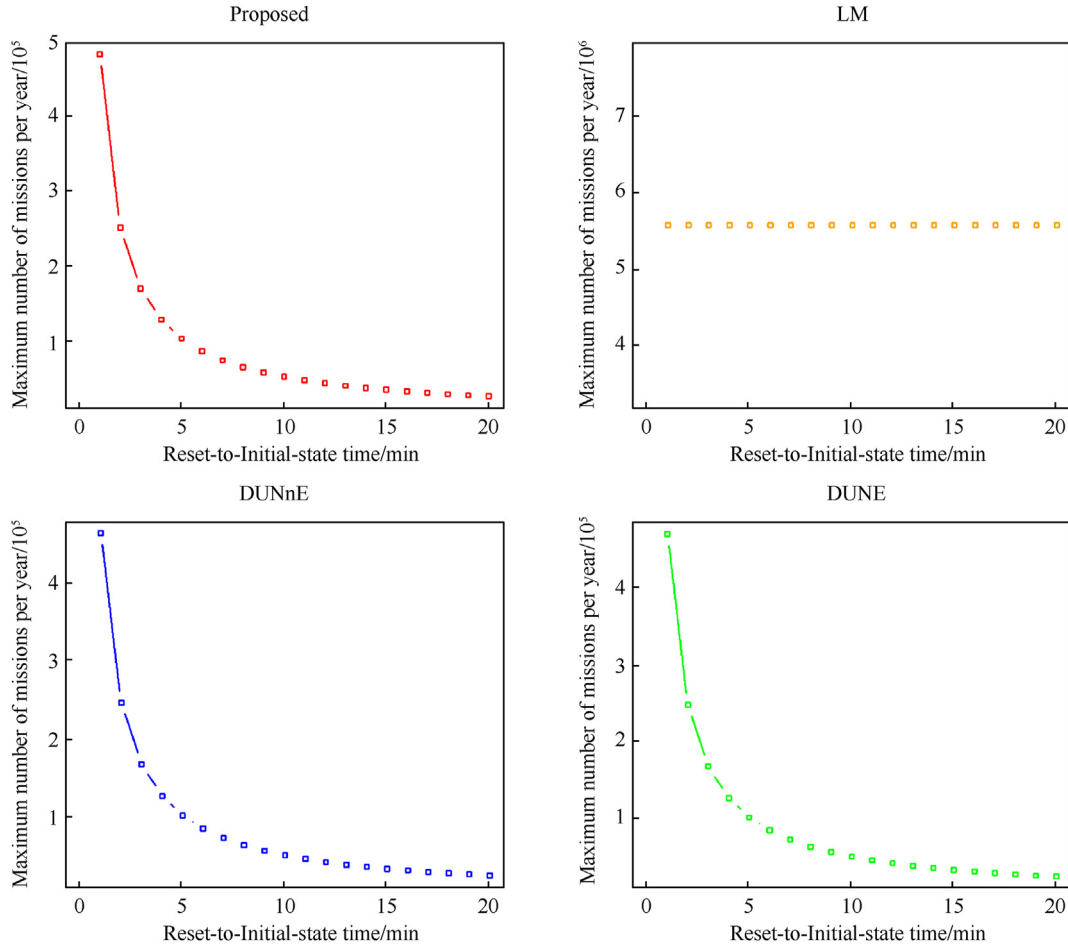
A.N. Skraparlis, K.S. Ntalianis and N. Tsapatsoulis

Fig. 9. Maximum number of missions per year for different reset-to-initial-state times.

to 600 m. For more than 600 m the proposed scheme provides better performance and (d) in cases of M_2 and M_1 LM performs better for initial distances up to 550 m. For more than 550 m the proposed scheme provides better performance. Overall, the proposed scheme provides an average time to neutralize target of 5.27 s, while LM provides 5.66 s, DUNnE provides 8.16 s and DUNE provides 7.16 s respectively. Thus, on average, the proposed scheme needs less time to neutralize the target, even though LM explodes when it approaches the target to less than 5 m. This is due to the fact that the proposed scheme incorporates the proposed innovative method to estimate the optimal points of interception (Fig. 4 and Eq. (54)), while LM, DUNnE and DUNE follow the tail of the target (full trajectory). As a result, on average, the proposed scheme provides a time reduction of 6.89%, 35.42% and 26.4% compared to LM, DUNnE and DUNE respectively, in case the target is on free fall with air resistance.

Regarding the operational capacity of each scheme, the maximum number of missions per year is estimated. More specifically, it is assumed that a mission starts at $t = 0$ (bomb release) and ends when dU_1 and dU_2 are ready for the next take-off. The total time or reset-to-initial-state time (T_t) includes the time to take-off and approach targets (t_{ap}), the time to neutralize targets (t_n), the time to land at the safe area (t_{ln}), the time to fill up fuel (t_{fl}) and the time to be put on the launcher for the next launch (t_l):

$$T_t = t_{ap} + t_n + t_{ln} + t_{fl} + t_l \tag{56}$$

If we set

$$T_r = t_{ap} + t_{ln} + t_{fl} + t_l \tag{57}$$

Then T_t can be written as

$$T_t = T_r + t_n \tag{58}$$

Additionally, t_n is replaced by the average time to neutralize targets, which has been previously estimated (Fig. 8) and

$$ET_r = \{T_r \in \mathbb{N} : 1 \le T_r \le 20\} \tag{59}$$

where ET_r is the set of the different integer values that T_r receives. In the following results, the minimum value is 1 min and the maximum is 20 min. Fig. 9 illustrates the maximum number of missions per year for the four compared schemes.

As it can be observed: (a) LM provides a fixed maximum number of missions per year (5,571,731), since T_r equals to zero. However, since the DDs explode, the new mission should be carried out by a new couple of DDs in case of LM (b) for the proposed approach and in case of $T_r = 1$, the maximum number of missions per year is 483,162, while for $T_r = 20$, the maximum number of missions per year falls to 26,165, (c) for DUNnE and in case of $T_r = 1$, the maximum number of missions per year is 462,676, while for $T_r = 20$, the maximum number of missions per year falls to 26,102 (d) finally for DUNE and in case of $T_r = 1$, the maximum number of missions per year is 469,565, while for $T_r = 20$, the maximum number of missions per year falls to 26,124. On average, the

A.N. Skraparlis, K.S. Ntalianis and N. Tsapatsoulis

proposed scheme reaches 91,089 maximum missions per year, while DUNnE and DUNE reach 89,364 and 89,948 maximum missions per year respectively. As a result, on average, the proposed scheme provides a maximum mission increase of 1.93% and 1.27% compared to DUNnE and DUNE respectively.

In the last experiment, the cost for different numbers of attacks is estimated for all schemes. Towards this direction let us assume that each DD has a weight of 10 kg and costs 10,000 Euros [73], except of the DD in case of LM, which costs 4000 Euros [74]. A lower cost is assumed, since in case of LM, the DD explodes and thus, it does include all special components that the DDs of the other three approaches are equipped with. Additionally, it is assumed that the DDs fly at top speed (444 km/h − 20% less than [64]). Let us also recall that the proposed scheme provides an average time to neutralize target of 5.27 s, while LM provides 5.66 s, DUNnE provides 8.16 s and DUNE provides 7.16 s respectively. Furthermore, let us assume that the rest of the mission (take-off, chase, land) requires 20 s on average, except in case of LM, which requires 10 s on average, since DDs do not land. Thus, on average, the total mission time is 25.27 s for the proposed scheme, 15.66 s for LM, 28.16 s for DUNnE and 27.16 s for DUNE. The major costs of each mission are: (a) the cost of buying the DDs, in case of LM and (b) the cost of the consumed fuel in all cases. In this paper, the theoretical thrust-specific fuel consumption (TSFC) [75,76] is adopted, were different TSFCs (different fuel efficiencies) are considered from 0.5 to 2.

Thrust is a mechanical force, generated through accelerating a mass of gas. The gas is propelled rearward, causing the engine to accelerate in the opposite direction [77]. In our case, each DD should produce a thrust to overcome two forces: (a) the weight force (Eq. (9)) and (b) the drag force Eqs. (6) and (28)). Thus

$$Th_d = m_d g + \frac{1}{2}\rho_a C_d A_b (u_d^{max})^2 \qquad (60)$$

where Th_d is the thrust, m_d is the mass and u_d^{max} is the top speed of the DD. Here it should be mentioned that Th_d is estimated for u_d^{max}. It should also be mentioned that it fluctuates based not only on the speed but also on the acceleration of the DD. However, Eq. (60) provides a good estimate of thrust, for a large part of the mission. Based on Eq. (60), Th_d = 233.23 N = 23.78 kg (force). Then, for example, if $TSFC$ = 1.0/2.0 then each DD needs 23.78/47.56 kg of fuel per hour (66.1/132.2 g/s). Raytheon Coyote Block 2 consumes JP-10 (exo-tetrahydrodicyclopentadiene, C10−H16), which is a synthetic aviation turbine fuel with an estimated cost of about 5300 Euro per ton (0,53 cents/g) [78]. Considering 10 missions per day on average,
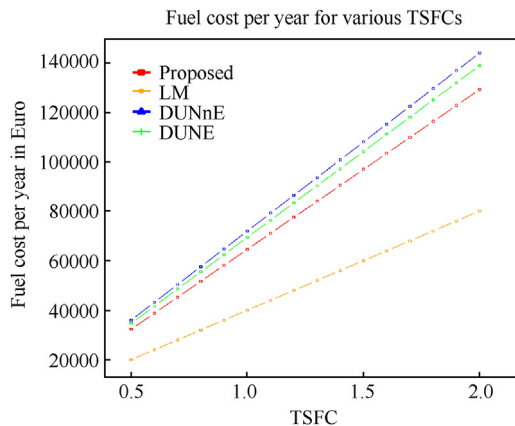
to protect all the CIs of a country, the total number of missions per year is 3650. Fig. 10 illustrates the fuel cost per year for the compared schemes and for different TSFCs (from 0.5 to 2.0). As it can be observed, the minimum fuel cost per year (20,024.5 Euro) is achieved by LM, for $TSFC$ = 0.5, while the maximum fuel cost (144,033.3 Euro) is achieved by DUNnE, for $TSFC$ = 2.0. On average, the proposed scheme achieves a fuel cost of 80,782.2 Euro, while LM, DUNnE and DUNE achieve 50,061.3 Euro (38.03% less than the proposed), 90,020.8 Euro (11.44% more than the proposed) and 86,824 Euro (7.48% more than the proposed) respectively. Here it should be mentioned that LM provides lower fuel costs, since the DDs explode and thus, they do not land at a safe area, as it happens with the other schemes.

Finally, in order to take into consideration also the cost of buying the DDs, let us assume that each DD has an operating life of 1000 missions. In other words, after this threshold, the DD is withdrawn from operation. Additionally, in case of LM, in each mission two DDs are destroyed. Furthermore, it is assumed that there are not any other maintenance costs during the span of the operating life of the DDs.

Fig. 11 illustrates the total cost in Euro per 1000 missions for different TSFCs (from 0.5 to 2.0). As it can be observed, the minimum total cost (18,852.8 Euro) is achieved by the proposed scheme for $TSFC$ = 0.5, while the maximum total cost (8,021,944.7 Euro) is achieved by LM for $TSFC$ = 2.0. On average, the proposed scheme achieves a total cost of 32,132.1 Euro, while LM, DUNnE and DUNE achieve 8,013,715.4 Euro (24,839.91% more than the proposed), 34,663.2 Euro (7.88% more than the proposed) and 33,787.4 Euro (5.15% more than the proposed) respectively. It is obvious that the total cost of LM is extremely high and other solutions should be examined. For example, instead of exploding near the target, the DDs could fire projectiles [46] or rockets [79]. Finally, it should be stated that the proposed scheme provides an average cost of 32.13 Euro per mission, which is very reasonable if we take into consideration that multi-million CIs are protected.

6. Discussion and future work

Before closing this paper, some interesting aspects are discussed. The first is related to the number of required DDs to neutralize malicious drones. In particular, the proposed method requires 2 DDs for 1 malicious bomb-carrying, kamikaze drone. The malicious bomb-carrying, kamikaze drone is also rigged with explosives. If the malicious kamikaze drone and/or the bomb hit the CI they may cause severe damage. Thus, both the malicious kamikaze drone and the bomb should be neutralized. In other words, 2 DDs neutralize 2 threats, leaving a "clear ground" i.e. scattered fragments, remains, or pieces do not fall on the ground. In the ideal case, the malicious bomb-carrying, kamikaze drone does not release the bomb. In this case dU_1 is enough to neutralize the threats without the need of dU_2. However, this case is very unlike. Additionally, when a malicious bomb-carrying, kamikaze drone approaches a CI, no one can guarantee that it will not release the bomb. If the bomb is released, there are two "clear ground" options, using the minimum number of DDs: (a) the proposed approach and (b) another approach that uses only one DD, e.g. dU_1. In the latter approach, dU_1 should capture the malicious kamikaze drone and then capture the bomb or capture the bomb and then the malicious kamikaze drone, before they reach the ground. Let us assume that dU_1 first captures the bomb and then chases the malicious kamikaze drone. If the captured bomb is detonated, it may destroy dU_1 and then the malicious kamikaze drone can head to the undefended CI. In any case, the latter approach needs further examination and triggers future research.

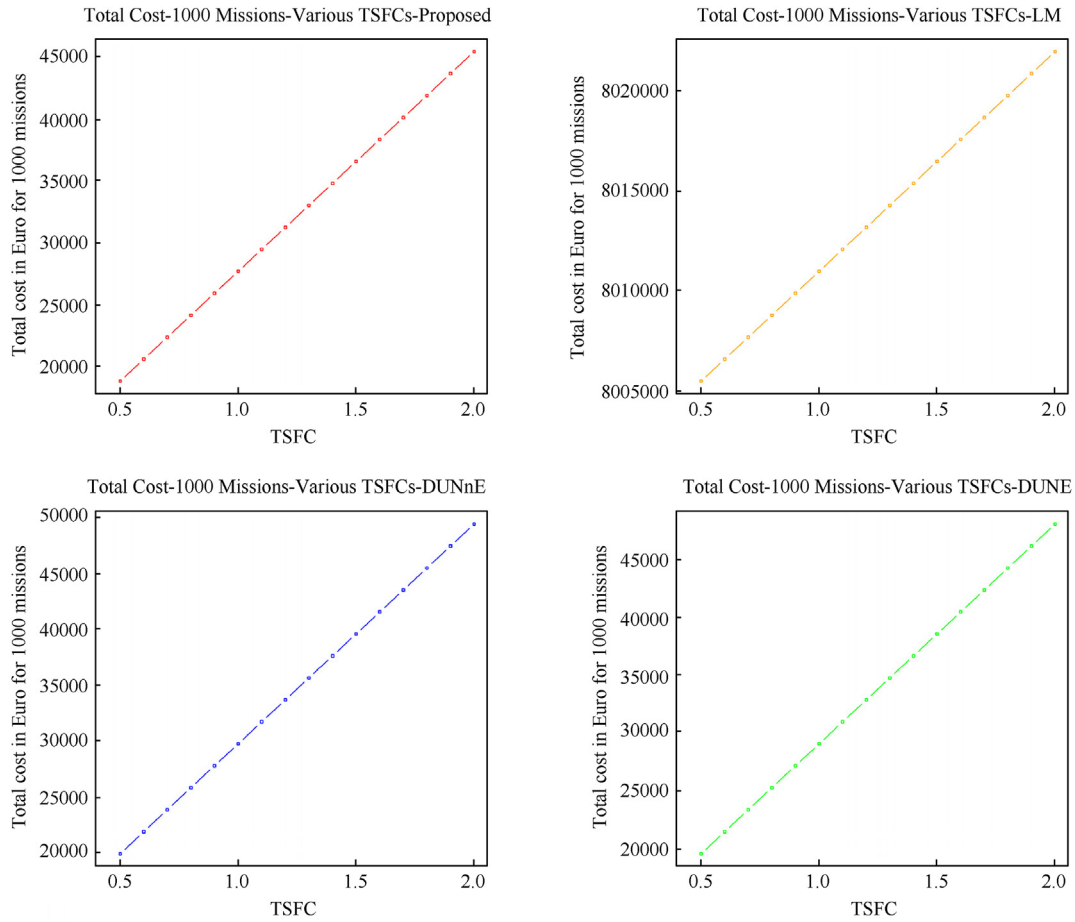On the other hand, according to Eq. (56) of the paper, the

Fig. 10. Fuel cost in Euro per year for the various schemes.

A.N. Skraparlis, K.S. Ntalianis and N. Tsapatsoulis

Fig. 11. Total cost in Euro per 1000 missions for the various schemes.

minimum total time of the proposed scheme (T_t) is 65.27 s ($T_r = 60$ s, $t_n = 5.27$ s). In this case, if a swarm of consecutive malicious bomb-carrying, kamikaze drones arrive one-by-one at least every 65.27 s, then dU_1 and dU_2 can neutralize all of them. Thus, only 2 defensive drones (dU_1 and dU_2) are enough to protect the CI from a swarm of many consecutive malicious bomb-carrying, kamikaze drones. Another very interesting scenario that can be the focus of future research, is the case of a swarm of many non-consecutive malicious bomb-carrying, kamikaze drones that approach the CI all-together. In this case, the minimum horizontal interception distance can be increased (leading possibly to more false alarms). In any case, this scenario also triggers much future research.

It should also be stressed that Israel's Iron Dome and Raytheon Coyote Block 3 with EMP may efficiently confront the swarm of many non-consecutive malicious bomb-carrying, kamikaze drones, but they do not leave a "clear ground", a factor that is important in urban areas, where people and property should also be protected from sky-falling debris.

The second aspect focuses on behavioral changes of the kamikaze drones. More specifically: what happens if the kamikaze drones change their preset autonomous navigation algorithms when they detect a DD is approaching? Or what if the kamikaze drones change their goal of achieving maximum damage?

Changing of the kamikaze drones' preset autonomous navigation algorithms when they detect an approaching DD, is a very interesting case. The DDs surveil a specific geographical region (3D spatial volume) around the CI, the borders of which are determined by the minimum take-off distance, as described in the paper. If the kamikaze drone crosses the border of the 3D spatial volume and continuous moving inside this volume, the DDs take-off and neutralize the kamikaze drone and the bomb. However, if the kamikaze drone enters the 3D spatial volume and after the DDs take-off the kamikaze drone exits the 3D spatial volume, this is a problem that needs to be analyzed in future research. Should the DDs intercept any drone even outside the 3D spatial volume, just because it has entered (maybe by mistake) the 3D spatial volume and exited before being neutralized? Should the DDs intercept drones even outside the 3D spatial volume, because they continuously enter and exit the volume (probably testing the protection algorithms of the DDs)? This case includes different subcases: (a) a testing-drone enters and exits the 3D spatial volume once (b) a testing-drone enters and exits the 3D spatial volume once and repeats this process after times t_1, t_2, t_3, etc., (c) a swarm of drones enter and exit the 3D spatial volume once, (d) a swarm of drones enter and exit the 3D spatial volume once and repeat this process after times t_1, t_2, t_3, etc. In these cases, probably drone-authentication methods should be incorporated to detect and confront testing-drones. In all cases, the DDs take-off, meaning that they consume fuel, their time until next service reduces and the CI may be vulnerable if it is attacked by the opposite direction.

On the other hand, changing of the kamikaze drones' goal of achieving maximum damage is another very interesting case. According to the proposed scheme, the DDs are programmed to take-off at the right moment to prevent any damage of the CI (minimum take-off distance from the CI, which determines the borders of the

3D spatial volume under surveillance). Even if the kamikaze drones' goal changes, they cannot approach the CI at a distance that will enable them to cause damage. Of course, a kamikaze drone can release the bomb at any time or can crash at any other location. However, in this case the bomb/kamikaze drone will not damage the CI, but may harm people and damage properties (houses, cars etc.) that are nearby the CI. It is very important to protect people and properties and future work should be carried out to examine schemes that can protect a whole city, leaving — at the same time — a "clear ground".

Future work can also focus on the case of very large payloads that cannot be effectively tackled by nets. Furthermore, another interesting case is when the kamikaze drone carries several releasable bombs. Additionally, CI-optimized security plans could be implemented, since each CI has different characteristics (size, dimensions, number of sensitive locations, level of importance, surrounding area etc.).

Finally, it should be mentioned that it is more practical to consider the drones' trajectories in 3 dimensions, even though the 2D motion provides a solution without loss of generality. The main reasons to consider 2D motion in this paper were to save space, use less formulas and less symbols, since the motions on x and z planes are described by similar mathematics.

7. Conclusions

CIs can be rapidly eliminated at a minimal expense, if aerial threats are not efficiently confronted. This work focused on the novel and under-researched field of neutralizing a fully autonomous, GPS-denied, bomb-carrying, non-military kamikaze drone. Towards this direction, this paper introduced the defensive couple of drones, which were equipped with a net-gun, with an innovative point-of-interception computational method and with an electromagnetic pulse weapon. Extensive results and comparisons to state-of-art methods, exhibited the advantages and limitations of the proposed scheme and triggered future work.

Declaration of competing interest

The authors declare that they have no known competing financial interests or personal relationships that could have appeared to influence the work reported in this paper.

Acknowledgment

References

[1] Krane J, Finley M. The US response to attacks on Persian gulf oil infrastructure and strategic implications for petro-states. Houston, Texas: Rice University's Baker Institute for Public Policy 2019. https://doi.org/10.25613/FF9S-SK08. vIssue brief no. 10.29.19.

[2] https://www.cnbc.com/2023/01/29/iran-reports-drone-attack-on-defense-facility.html. [Accessed 26 January 2024].

[3] Wendt P, Voltes-Dorta A, Suau-Sanchez P. Estimating the costs for the airport operator and airlines of a drone-related shutdown: an application to Frankfurt international airport. J Transp Secur 2020;13:93—116. https://doi.org/10.1007/s12198-020-00212-4.

[4] Skraparlis A, Ntalianis KS, Mastorakis NE. Real time threat assessment of truck Cargos carrying dangerous goods for preventing terrorism attacks on neighboring critical infrastructures. IEEE Access 2022;10:76547—62. https://doi.org/10.1109/ACCESS.2022.3189674.

[5] Park S, Kim HT, Lee S, Joo H, Kim H. Survey on anti-drone systems: components, designs, and challenges. IEEE Access 2021;9:42635—59. https://doi.org/10.1109/ACCESS.2021.3065926.

[6] Lees FP. Loss prevention in the process industries: hazard identification,

[7] assessment and control. second ed. Butterworth-Heinemann; 1996.

[7] https://en.wikipedia.org/wiki/TNT_equivalent, Retrieved: 26 January 2024.

[8] Dewey JM. Studies of the TNT equivalence of propane, propane/oxygen, and ANFO. Shock Waves 2020;30:483—9. https://doi.org/10.1007/s00193-020-00949-w.

[9] Török Z, Ozunu A. Hazardous properties of ammonium nitrate and modeling of explosions using TNT equivalency. Environ Eng Manag J 2015;14(11): 2671—8. https://doi.org/10.30638/eemj.2015.284.

[10] Bjerketvedt D, Bakke JR, van Wingerden K. Gas explosion handbook. Available online at: https://www.gexcon.com/wp-content/uploads/2020/08/Gas-Explosion-Handbook-1992-version-new-front-page-2019.pdf; 2019. Retrieved: 26 January 2024.

[11] Ullah A, Ahmad F, Jang H-W, Kim S-W. Review of analytical and empirical estimations for incident blast pressure. KSCE J Civ Eng December 2016:1—15.

[12] Hopkinson B. British ordnance board minutes. Rep 1915;13565.

[13] Cranz C. Lehrbuch der Ballistik, II Band. Berlin. 1926.

[14] Kinney GF, Graham KJ. Explosive shocks in air. Berlin and New York: Springer-Verlag; 1985.

[15] Eyes of the Army, U.S. Army roadmap for unmanned aircraft systems 2010 — 2035. U.S. Army UAS Center of Excellence, Available Online: https://irp.fas.org/program/collect/uas-army.pdf. Retrieved: 26 January 2024.

[16] Cary L, and Coyne J. "ICAO Unmanned Aircraft Systems (UAS), Circular 328," 2011—2012 UAS Yearbook — UAS: The Global Perspective. Blyenburgh & Co. pp. 112—115. Available Online: https://web.archive.org/web/20160304025432/http://uvs-info.com/phocadownload/05_3a_2011/P112-P115_C%26AI_ICAO-Advisory-Circular.pdf, Retrieved: 26 January 2024.

[17] Hu J, Lanzon A. An innovative tri-rotor drone and associated distributed aerial drone swarm control. Robot Autonom Syst 2018;103:162—74. https://doi.org/10.1016/j.robot.2018.02.019.

[18] https://www.insidehook.com/gear/griff-800-lifting-drone, Retrieved: 26 January 2024.

[19] https://evtol.news/zhuhai-svffi-aviation-sf-dl-180, Retrieved: 26 January 2024.

[20] https://www.alibaba.com/product-detail/50Kg-payload-professional-transport-drone-for_1600747623532.html?spm=a2700.galleryofferlist.normal_offer.d_title.27559bd59G115Q, Retrieved: 26 January 2024.

[21] https://www.alibaba.com/product-detail/JT16L-404QC-smart-granule-spreader-drone_1600305044921.html, Retrieved: 26 January 2024.

[22] https://makezine.com/article/maker-news/goliath-the-gas-powered-quadcopter/, Retrieved: 26 January 2024.

[23] https://www.onyxstar.net/hydra-12/, Retrieved: 26 January 2024.

[24] https://www.yangdaonline.com/yangda-sky-whale-heavy-lift-long-endurance-electric-vtol-drone/, Retrieved: 26 January 2024.

[25] https://freeflysystems.com/alta-x, Retrieved: 26 January 2024.

[26] https://enterprise.dji.com/matrice-300, Retrieved: 26 January 2024.

[27] https://www.drl.io/racerx, Retrieved: 26 January 2024.

[28] Dudenhoeffer DD. Day of the drone: protecting critical infrastructure from terrorist use of unmanned aerial systems. In: Toward effective cyber defense in accordance with the rules of law. IOS Press; 2020. p. 17—31. https://doi.org/10.3233/NHSDP20038.

[29] Schneider M, Lichte D, Witte D, Gimbel S, Brucherseifer E. Scenario analysis of threats posed to critical infrastructures by civilian drones. In: Proceedings of the 31st European safety and reliability conference. Research Publishing Services; 2021.

[30] Valianti P, Papaioannou S, Kolios P, Ellinas G. Multi-agent coordinated close-in jamming for disabling a rogue drone. IEEE Trans Mobile Comput 2022;21(10): 3700—17. https://doi.org/10.1109/TMC.2021.3062225.

[31] Souli N, Kolios P, Ellinas G. Multi-agent system for rogue drone interception. IEEE Rob Autom Lett April 2023;8(4):2221—8. https://doi.org/10.1109/LRA.2023.3245412.

[32] Kim I, Lee H-Y, Lee D-M, Lee H-J, Kim H, Kim E-S, Kim N-Y. Broadband gain enhanced narrow-beam Vivaldi antenna with ring and directors for handheld antidrone jamming system. In: IEEE Antenn Wireless Propag Lett; 2023. https://doi.org/10.1109/LAWP.2023.3321899.

[33] Slimeni F, Delleji T, Chtourou Z. RF-based mini-drone detection, identification & jamming in No fly zones using software defined radio. In: Nguyen NT, Manolopoulos Y, Chbeir R, Kozierkiewicz A, Trawinski B, editors. Computational collective intelligence. Lecture notes in computer science, vol vol. 13501.. Cham: ICCCI; 2022. https://doi.org/10.1007/978-3-031-16014-1-62.

[34] Abunada AH, Osman AY, Khandakar A, Chowdhury MEH, Khattab T, Touati F. Design and implementation of a RF based anti-drone system. Doha, Qatar. In: 2020 IEEE international conference on informatics, IoT, and enabling technologies (ICIoT); 2020. p. 35—42. https://doi.org/10.1109/ICIoT48696.2020.9089515.

[35] Balachandran V, Chua M. Neutralizing hostile drones with surveillance drones. In: Codaspy '21: proceedings of the eleventh ACM conference on data and application security and privacy; 2021. p. 297—9. https://doi.org/10.1145/3422337.3450318.

[36] Chiper FL, Martian A, Vladeanu C, Marghescu I, Craciunescu R, Fratu O. Drone detection and defense systems: survey and a software-defined radio-based solution. MDPI Sensors 2022;22(4). https://doi.org/10.3390/s22041453.

[37] Ferreira R, Gaspar J, Sebastião P, Souto N. A software defined radio based anti-UAV mobile system with jamming and spoofing capabilities. MDPI Sensors 2022;22(4). https://doi.org/10.3390/s22041487.

[38] Razooqi OD, Ali AH. Drones neutralized by utilize electromagnetic pulse (EMP)

system. In: 2022 5th international conference on engineering technology and its applications (IICETA), Al-Najaf, Iraq; 2022. p. 487—92. https://doi.org/10.1109/IICETA54559.2022.9888673.

[39] Zhao S, Xie R, Wan J. Design of anti-drone laser weapon systems. In: SPIE/COS Photonics Asia, vol. 11544, High-Power Lasers and Applications XI; 115440A; 2020. https://doi.org/10.1117/12.2575171.

[40] Edwards DM. "Simulated laser weapon system decision support to combat drone swarms with machine learning," Master's Thesis, Naval Postgraduate School Monterey CA, September 2021, Accession Number: AD1164253.

[41] González F, Caballero R, Pérez-Grau FJ, Viguria A. Vision-based UAV detection for air-to-air neutralization. In: 2021 IEEE international symposium on safety, security, and rescue robotics (SSRR), New York City, NY, USA; 2021. p. 236—41. https://doi.org/10.1109/SSRR53300.2021.9597861.

[42] Liu Z, Mucchiani C, Ye K, Karydis K. Safely catching aerial micro-robots in mid-air using an open-source aerial robot with soft gripper. Front Robot AI, Bio-Inspired Robot 2022;9. https://doi.org/10.3389/frobt.2022.1030515.

[43] García M, Viguria A, Heredia G, Ollero A. Minimal-Time Trajectories for Interception of Malicious Drones in Constrained Environments. In: Tzovaras D, Giakoumis D, Vincze M, Argyros A, editors. Computer Vision Systems. Lecture Notes in Computer Science, vol. vol. 11754.. Cham: ICVS; 2019. https://doi.org/10.1007/978-3-030-34995-0-67.

[44] García M, Caballero R, González F, Viguria A, Ollero A. Autonomous drone with ability to track and capture an aerial target. In: 2020 international conference on unmanned aircraft systems (ICUAS), Athens, Greece; 2020. p. 32—40. https://doi.org/10.1109/ICUAS48674.2020.9213883.

[45] Wyder PM, Chen Y-S, Lasrado AJ, Pelles RJ, Kwiatkowski R, Comas EOA, Kennedy R, Mangla A, Huang Z, Hu X, Xiong Z, Aharoni T, Chuang T-C, Lipson H. Autonomous drone hunter operating by deep learning and all-onboard computations in GPS-denied environments. PLoS One 2019;14(11): e0225092. https://doi.org/10.1371/journal.pone.0225092.

[46] Robbe C, Papy A, Nsiampa N. Using kinetic energy non-lethal weapons to neutralize low small drone unmanned aerial vehicles. vol. 2. In: Human Factors and Mechanical Engineering for Defense and Safety; 2018. https://doi.org/10.1007/s41314-018-0008-y.

[47] Chen Y, Li Z, Li L, Ma S, Zhang F, Fan C. An anti-drone device based on capture technology. Biomim Intell Robot 2022;2(3). https://doi.org/10.1016/j.birob.2022.100060.

[48] Rothe J, Strohmeier M, Montenegro S. A concept for catching drones with a net carried by cooperative UAVs. In: 2019 IEEE international symposium on safety, security, and rescue robotics (SSRR), Würzburg, Germany; 2019. p. 126—32. https://doi.org/10.1109/SSRR.2019.8848973.

[49] Fedoseev A, Serpiva V, Karmanova E, Cabrera MA, Shirokun V, Vasilev I, Savushkin S, Tsetserukou D. DroneTrap: drone catching in midair by soft robotic hand with color-based force detection and hand gesture recognition. In: 2021 IEEE 4th international conference on soft robotics (RoboSoft), New Haven, CT, USA; 2021. p. 261—6. https://doi.org/10.1109/RoboSoft51838.2021.9479353.

[50] Wang J, Zhao L, Xia K. A discrete-time intercepting strategy for net capture using multiple unmanned aerial vehicles. In: 2022 IEEE international conference on unmanned systems (ICUS), Guangzhou, China; 2022. p. 430—5. https://doi.org/10.1109/ICUS55513.2022.9986777.

[51] Yang K, Quan Q. An autonomous intercept drone with image-based visual servo. In: 2020 IEEE international conference on robotics and automation (ICRA), Paris, France; 2020. p. 2230—6. https://doi.org/10.1109/ICRA40945.2020.9197539.

[52] Tao H, Song T, Lin D, Jin R, Li B. Autonomous navigation and control system for capturing a moving drone. Field Robot 2022;2:34—54.

[53] Lyu C, Zhan R. Global analysis of active defense technologies for unmanned aerial vehicle. IEEE Aero Electron Syst Mag 2022;37(1):6—31. https://doi.org/10.1109/MAES.2021.3115205.

[54] Swinney CJ, Woods JC. A review of security incidents and defence techniques relating to the malicious use of small unmanned aerial systems. IEEE Aero Electron Syst Mag 2022;37(5):14—28. https://doi.org/10.1109/MAES.2022.3151308.

[55] Kang H, Joung J, Kim J, Kang J, Cho YS. Protect your sky: a survey of counter unmanned aerial vehicle systems. IEEE Access 2020;8:168671—710. https://doi.org/10.1109/ACCESS.2020.3023473.

[56] Chamola V, Kotesh P, Agarwal A, Naren, Gupta N, Guizani M. A comprehensive review of unmanned aerial vehicle attacks and neutralization techniques. Ad Hoc Netw February 2021;111. https://doi.org/10.1016/j.adhoc.2020.102324.

[57] Pärlin K, Riihonen T, Le Nir V, Adrat M. Physical-layer reliability of drones and their counter-measures: full vs. Half duplex," in. IEEE Trans Wireless Commun 2023. https://doi.org/10.1109/TWC.2023.3290257.

[58] Husodo AY, Jati G, Octavian A, Jatmiko W. Switching target communication strategy for optimizing multiple pursuer drones performance in immobilizing Kamikaze multiple evader drones. ICT Express 2020;6(2):76—82. https://doi.org/10.1016/j.icte.2020.03.007.

[59] Lefebvre T, Dubot T, Joulia A. Conceptual study of an Anti-Drone Drone through the coupling of design process and interception strategy simulations. In: 16th AIAA aviation technology, integration, and operations conference, Washington, D.C; 2016.

[60] Goppert JM, Wagoner AR, Schrader DK, Ghose S, Kim Y, Park S, Gomez M, Matson ET, Hopmeier MJ. Realization of an autonomous, air-to-air counter unmanned aerial system (CUAS). In: 2017 first IEEE international conference on robotic computing (IRC), Taichung, Taiwan, China; 2017. p. 235—40. https://doi.org/10.1109/IRC.2017.10.

[61] Wilson EB. Bomb trajectories. Report no. 79, National Advisory Committee for Aeronautics. Washington Government Printing Office; 1920. Available Online: https://ntrs.nasa.gov/citations/19930091140. Retrieved: 26 January 2024.

[62] Parker GW. Projectile motion with air resistance quadratic in the speed. Am J Phys 1977;45(7):606—10. https://doi.org/10.1119/1.10812.

[63] https://www.unmannedairspace.info/counter-uas-systems-and-policies/us-army-tests-raytheons-coyote-block-3-non-kinetic-counter-drone-device-de-feats-swarm-of-drones/, Retrieved: 26 January 2024.

[64] https://www.thedrive.com/the-war-zone/22223/army-buys-small-suicide-drones-to-break-up-hostile-swarms-and-potentially-more, Retrieved: 26 January 2024.

[65] Jao JK. Coherent multilateral radar processing for precise target geolocation. In: 2006 IEEE conference on radar, Verona, NY, USA; 2006. p. 6. https://doi.org/10.1109/RADAR.2006.1631819.

[66] https://www.nrcs.usda.gov/wps/portal/nrcs/detail/null/?cid=nrcs144p2_056386, Retrieved: 26 January 2024.

[67] https://aiimpacts.org/discontinuity-from-nuclear-weapons/, Retrieved: 26 January 2024.

[68] https://chemistry.illinois.edu/system/files/inline-files/8_LaFrate_Abstract_SP05.pdf., Retrieved: 26 January 2024.

[69] https://www1.grc.nasa.gov/beginners-guide-to-aeronautics/enginesimu/, Retrieved: 26 January 2024.

[70] Voskuijl M. Performance analysis and design of loitering munitions: a comprehensive technical survey of recent developments. Defence Technol 2022;18(3):325—43. https://doi.org/10.1016/j.dt.2021.08.010.

[71] Mishra A, Bajpai A, Mishra A, Mishra A. Autonomous defence vehicle for precise targeting and mission accomplishment — a survey of various technologies. In: 2020 international conference on smart electronics and communication (ICOSEC), Trichy, India; 2020. p. 1184—91. https://doi.org/10.1109/ICOSEC49089.2020.9215320.

[72] Wang H, Lin D -f, Wang J, Cheng Z -x. Study on homing guidance systems based on different source errors. In: 2010 international conference on computer, mechatronics, control and electronic engineering, Changchun, China; 2010. p. 118—21. https://doi.org/10.1109/CMCE.2010.5609891.

[73] https://www.thedrive.com/the-war-zone/22223/army-buys-small-suicide-drones-to-break-up-hostile-swarms-and-potentially-more, Retrieved: 26 January 2024.

[74] https://www.navair.navy.mil/node/7931, Retrieved: 26 January 2024.

[75] https://ntrs.nasa.gov/api/citations/19770021179/downloads/19770021179.pdf, Retrieved: 26 January 2024.

[76] https://www.grc.nasa.gov/www/k-12/airplane/sfc.html, Retrieved: 26 January 2024.

[77] https://www.grc.nasa.gov/www/k-12/VirtualAero/BottleRocket/airplane/thrsteq.html, Retrieved: 26 January 2024.

[78] https://www.konochem.com/intermediates/top-qualtiy-99-exo-jp-10-exo.html, Retrieved: 26 January 2024.

[79] https://www.airforce-technology.com/news/greek-sas-technologys-sarisa-drone-successfully-fires-thales-70mm-rocket/?cf-view, Retrieved: 26 January 2024.